

# Pionic hydrogen and deuterium

D. Gotta<sup>1\*</sup> and L.M. Simons<sup>2</sup>

<sup>1</sup> Institut für Kernphysik, Forschungszentrum Jülich GmbH, D-52425 Jülich, Germany

<sup>2</sup> Paul Scherrer Institut, CH-5232 Villigen, Switzerland

\* d.gotta@fz-juelich.de

February 4, 2021

PAUL SCHERRER INSTITUT



Review of Particle Physics at PSI

doi:[10.21468/SciPostPhysProc.2](https://doi.org/10.21468/SciPostPhysProc.2)

## Abstract

The measurement of strong-interaction shift and broadening in pionic hydrogen and deuterium yields pion-nucleon scattering lengths as well as the threshold pion-production strength on isoscalar  $NN$  pairs. Results from recent high-resolution experiments at PSI using crystal spectrometers allow important comparisons with the outcome of the modern low-energy description of QCD within the framework of effective field theories.

## 14.1 Introduction

The last decades have seen a successful theoretical description of strong-interaction phenomena at threshold within effective field-theory (EFT) approaches: the chiral symmetry of the QCD Lagrangian allows the derivation of so-called low-energy theorems. In reality, the chiral symmetry is explicitly broken because of the finite masses of the light quarks  $u$ ,  $d$ , and  $s$ . This leads, *e.g.* to a finite pion mass which is, however, still small compared to the hadronic scale given by the nucleon mass. The deviations from low-energy theorems reveal the amount of symmetry breaking.

Chiral Perturbation Theory ( $\chi$ PT) offers a systematic way of quantifying these symmetry-breaking effects. A chiral expansion, ordered by the powers of (small) momenta, the quark-mass differences, and the fine structure constant  $\alpha$ , includes strong isospin-breaking effects resulting from the quark-mass differences and those of electromagnetic origin on the same footing. The unknown structure of QCD at short distances is parametrized by so-called low-energy constants (LECs), which must be taken from experiment as long as results from lattice-QCD calculations are not available.

Pions, being composite particles of the lightest quarks  $u$  and  $d$ , and their interactions, play a prominent role. Hence,  $\pi N \rightarrow \pi N$  reactions and the corresponding scattering lengths are of fundamental interest for the understanding of low-energy QCD phenomena. In the limit of isospin conservation, all  $\pi N \rightarrow \pi N$  reactions are completely determined by only two independent real numbers, the scattering lengths corresponding to the isospin combinations  $I = 1/2$  and  $3/2$  of the  $\pi N$  system. Therefore, quantitative tests of isospin-breaking effects, predicted to be of the order of a few per cent by advanced  $\chi$ PT calculations, are of great importance.

The corresponding precision for the experimental approach is achieved by means of high-resolution X-ray spectroscopy of pionic hydrogen and deuterium. Considering the energy regime of such atomic systems, the measurement of the strong-interaction effects constitutes a scattering experiment at threshold.

41 Concepts and recent theoretical efforts on low-energy  $\pi N$  scattering and pionic hydrogen  
 42 are reviewed in [1, 2]. Properties of exotic atoms and experimental methods are outlined  
 43 in [3].

## 44 14.2 Strong-interaction effects

45 Exotic atoms provide an ideal laboratory for the extraction of scattering lengths from experi-  
 46 ment, because problems due to normalization and extrapolation to threshold inherent to scat-  
 47 tering experiments are absent. Such atoms are formed when negatively charged particles,  
 48 such as pions, are captured in high-lying atomic levels of the Coulomb potential of a nucleus:  
 49 a de-excitation cascade subsequently starts. The strong interaction gives rise to a change of the  
 50 total energy of the particle-nucleus system  $\Delta E$  and to its lifetime observed as an energy shift  $\epsilon$   
 51 and a broadening  $\Gamma$  of lower-lying atomic levels, where the overlap of the atomic bound-state  
 52 wave function with the nucleus of mass number  $A$  becomes significant. For atomic states with  
 53 principle quantum number  $n$  and angular momentum  $\ell = 0$ ,  $ns$ , the complex energy shift is  
 54 directly related to the complex scattering length  $a_{\pi A}$  [4]

$$\Delta E_{ns}^{\pi A} - i \frac{\Gamma_{ns}^{\pi A}}{2} = -\frac{2\alpha^3 \mu_A^2 c^4}{\hbar c} \cdot \frac{1}{n^3} \cdot a_{\pi A} + \dots, \quad (14.1)$$

55 where  $\alpha$  is the fine structure constant and  $\mu_A$  is the reduced mass of the particle-nucleus system.  
 56 The ellipses stand for higher order corrections [1, 2]. In this paper, the sign convention for  
 57 atomic level shifts  $\epsilon$  is the change of the X-ray transition energy, *i. e.*  $\epsilon \equiv -\Delta E$ .

58 In the case of pionic hydrogen, only the ground-state effects are detectable by high-resolution  
 59 X-ray spectroscopy. The two independent scattering lengths may be described by isoscalar and  
 60 isovector scattering lengths  $a^+$  and  $a^-$  for the elastic channels:

$$a^\pm \equiv (a_{\pi^- p \rightarrow \pi^- p} \pm a_{\pi^+ p \rightarrow \pi^+ p}). \quad (14.2)$$

61  $a^+$  and  $a^-$  are given in term of the isospin combinations  $I = 1/2$  and  $I=3/2$  by:

$$a^+ = \frac{1}{3}(a_{1/2} + 2a_{3/2}) \quad \text{and} \quad (14.3)$$

$$a^- = \frac{1}{3}(a_{1/2} - a_{3/2}). \quad (14.4)$$

62 In leading order, pionic hydrogen and deuterium give access to the scattering lengths of the  
 63 elastic reactions  $\pi^- p \rightarrow \pi^- p$  and  $\pi^- n \rightarrow \pi^- n$  and to the charge exchange channel  $\pi^- p \rightarrow \pi^0 n$   
 64 after correcting for the radiative capture contribution  $\pi^- p \rightarrow \gamma n$ . As seen from (14.5) – (14.7),  
 65 three experimental quantities are available for the two independent scattering lengths: the 1s-  
 66 level strong-interaction shifts in pionic hydrogen and deuterium  $\epsilon_{1s}^{\pi H}$  and  $\epsilon_{1s}^{\pi D}$  and broadening  
 67 in pionic hydrogen,  $\Gamma_{1s}^{\pi H}$ . Hence, such measurements constitute a decisive constraint both on  
 68 the experimental and theoretical approaches.

$$\epsilon_{1s}^{\pi H} \propto \text{Re } a_{\pi^- p} \propto a_{\pi^- p \rightarrow \pi^- p} = a^+ + a^- + \dots \quad (14.5)$$

$$\Gamma_{1s}^{\pi H} \propto \Im a_{\pi^- p} \propto (a_{\pi^- p \rightarrow \pi^0 n})^2 = (a^-)^2 + \dots \quad (14.6)$$

$$\epsilon_{1s}^{\pi D} \propto \text{Re } a_{\pi^- d} \propto a_{\pi^- p \rightarrow \pi^- p} + a_{\pi^- n \rightarrow \pi^- n} = 2 \cdot a^+ + \dots \quad (14.7)$$

69 The ellipses indicate the corrections needed to derive the QCD quantities  $a^+$  and  $a^-$  from the  
 70 measurable quantities  $a_{\pi N \rightarrow \pi N}$ . These corrections are given by recent  $\chi$ PT calculations [1, 2].  
 71 For the pionic deuterium case, in addition substantial multi-body corrections are necessary  
 72 which, however, are well under control [5]. The check of consistency of these results is an  
 73 essential outcome of the experimental and theoretical efforts of the last decades.

74 The imaginary part  $\text{Im} a_{\pi D}$ , which gives the leading contribution to the hadronic broaden-  
 75 ing  $\Gamma_{1s}^{\pi D}$  in pionic deuterium, measures the transition strength  $\alpha$  of  $s$ -wave pions on an isoscalar  
 76 nucleon-nucleon pair  $\pi NN \leftrightarrow NN$  and is an independent quantity not related to the scattering  
 77 lengths  $a^+$  and  $a^-$  [6,7].

$$\Gamma_{1s}^{\pi D} \propto \Im a_{\pi-d} \propto \sigma_{\pi^+d \rightarrow pp}^{\text{threshold}} \propto \alpha \quad (14.8)$$

### 78 14.3 Experimental approach

79 The possibility of performing high-statistics experiments of exotic hydrogen even in dilute  
 80 targets with high-resolution devices like crystal spectrometers became possible by using the  
 81 cyclotron trap (Section ??). Figure 14.1 shows the set-up of cyclotron trap and crystal spec-  
 82 trometer for the studies described here [7–10]. With a massive specially tailored concrete  
 83 shielding an improvement in the beam-induced background of up to a factor of 50 is achieved  
 84 compared to previous experiments.

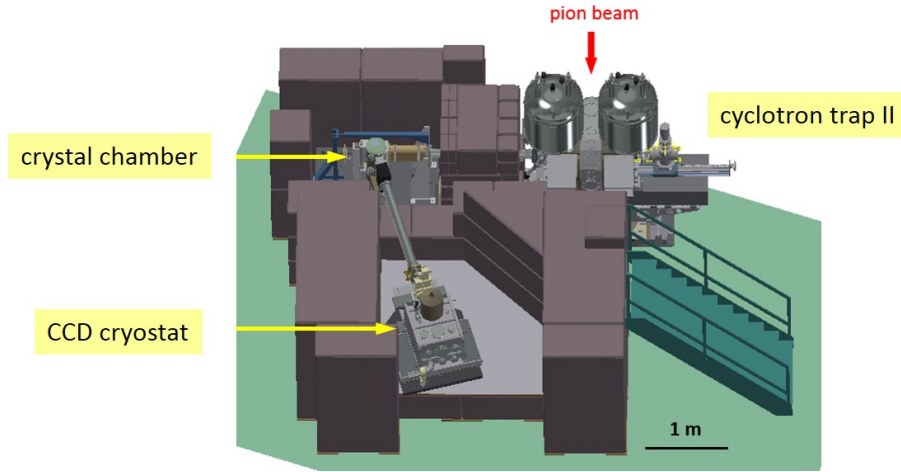


Figure 14.1: Set-up in the  $\pi E5$  area at PSI. The Bragg crystal is mounted inside a vacuum chamber and connected to the cyclotron trap and the CCD X-ray detector by a vacuum system to minimize absorption losses. The roof of the concrete cave is not shown.

85 The crystal spectrometer was set up in Johann configuration which allows the measure-  
 86 ment of an energy interval corresponding to the extension of the X-ray source in the direction  
 87 of dispersion [11]. Thin polished slabs of silicon and quartz were used as Bragg crystals. They  
 88 are spherically bent with radii of about  $R_c = 3$  m when attached to glass lenses of optical  
 89 quality by adhesive forces only (Figure 14.2). Resolutions of 270 – 460 meV were achieved  
 90 for the X-rays in the energy range of 2.2 – 3.1 keV which is very close to the theoretical limit  
 91 achievable for the particular crystal and reflection.

92 The detector extension in the direction of dispersion has to be matched to the source size  
 93 to utilize the capabilities of the Johann set-up. The detector is realized as a 2 x 3 array of  
 94 Charge-Coupled Device (CCD) of total area of 48 x 72 mm<sup>2</sup> (Figure 14.2) and located at the  
 95 distance  $R_c \cdot \sin \Theta_B$  given by the focussing condition where  $\Theta_B$  is the Bragg angle. The diffracted  
 96 X-rays create a cone-like hit pattern in the detection plane which, after curvature correction  
 97 and projection to the direction of dispersion, directly yields an energy spectrum (Figure 14.3).  
 98 The necessary two-dimensional position resolution is provided by the  $40 \mu\text{m} \times 40 \mu\text{m}$  pixel  
 99 structure of the CCDs.

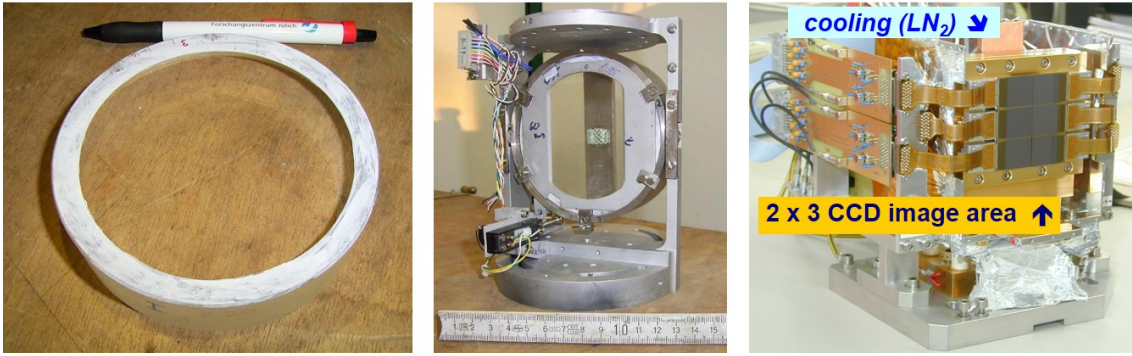


Figure 14.2: Left: quartz disk attached adhesively to a concave glass lens, middle: crystal mounting in an adjustable support frame with an aperture to limit the so-called Johann defocussing, right: focal-plane X-ray detector removed from the cryostat [12].

100 Energy determination in Johann-type set-ups requires a calibration line ideally at the same  
 101 Bragg angle as the X-ray line of interest. In this experiment, the energy of the pionic oxygen  
 102 line (6 – 5) is very close to the one of pionic hydrogen (3 – 1). The precise knowledge of the  
 103 charged pion mass then allows the calibration of pionic-atom transitions among themselves  
 104 [13] (Section 10 [14]).

105 The understanding of collisional processes during the lifetime of pionic hydrogen plays a  
 106 key role for a precision determination of the strong-interaction effects. For the  $\pi\text{H}$  system,  
 107 X-ray transition energies are of the order of 3 keV while hadronic shifts are of the order of  
 108 a few eV and the broadening around 1 eV. Therefore, a thorough study of possible collision-  
 109 induced energy shifts and broadening has been performed. Such a study essentially means the  
 110 measurement of various transitions at various target densities as well as a comparison with  
 111 muonic hydrogen. The hydrogen density was adjusted in the cryogenic target by temperature  
 112 variation in order to allow the use of thin windows.

113 Energy shifts, which would spoil the result for  $\epsilon_{1s}$ , may appear if after molecular forma-  
 114 tion  $\pi\text{H} + \text{H}_2 \rightarrow [(pp\pi)p]ee$  X-ray emission from molecular states occurs. As the formation  
 115 rate scales with collision probability, a density-dependent X-ray energy would demonstrate its  
 116 appearance. No such effect was observed for either hydrogen and deuterium [7–9].

117 The main obstacle to a precision determination of the hadronic broadening  $\Gamma_{1s}$  is Doppler  
 118 broadening due to Coulomb de-excitation. During these non-radiative transitions, the energy  
 119 of the de-excitation step ( $n - n'$ ) is transferred into kinetic energy of the collision partners. The  
 120 competition of acceleration by Coulomb de-excitation and deceleration by elastic and inelastic  
 121 collisions leads to a complex kinetic energy distribution at the time of X-ray emission. Hence,  
 122 the measured line shape is a convolution of spectrometer response, Doppler broadening, and  
 123 the Lorentzian representing the hadronic broadening. For that reason, a measurement of the  
 124 twin system muonic hydrogen was performed, where the absence of the strong interaction  
 125 allows the possibility of directly studying the effect of Doppler broadening.

126 Consequently, the ultimate knowledge of the spectrometer response is of great importance.  
 127 Here, the cyclotron trap offers another unique possibility when extended to operate as ECR  
 128 source (Section 13 [15]). The ECR source yields narrow X-rays at high rates from helium-like  
 129 low  $Z$  elements like sulphur, chlorine, and argon which almost coincide in energy with the  
 130 pionic hydrogen and deuterium X-ray transitions.

131 **14.4 Results**

132 Spectra of the  $(3p - 1s)$  transitions are shown in Figure 14.3. Above the oxygen freeze-out  
 133 temperature the simultaneous measurement of the  $\pi\text{O}$  calibration line and  $\pi\text{H}$  line is feasible  
 134 by means of a small  $\text{O}_2$  admixture to the  $\text{H}_2$  gas. For lower temperature, hydrogen and oxygen  
 135 measurements were performed alternately.

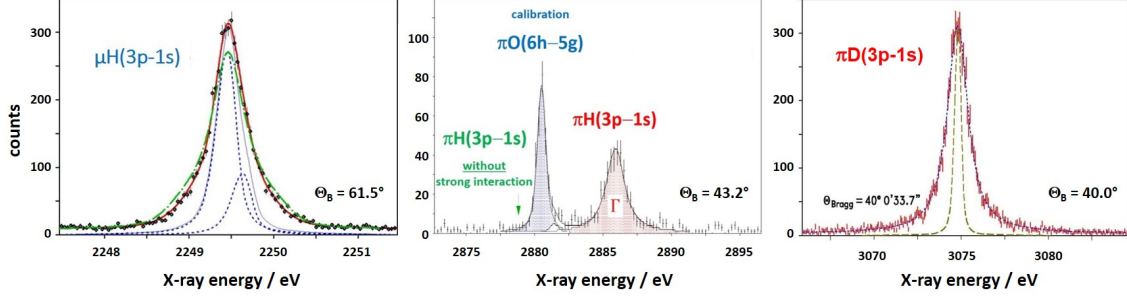


Figure 14.3: Spectra of the  $(3p - 1s)$  transitions in muonic [8] and pionic hydrogen [9] and pionic deuterium [7]. The narrow structures displayed inside the  $\mu\text{H}$  and  $\pi\text{D}$  lines demonstrate the resolution of the spectrometer equipped with a Si 111 crystal as measured by using an ECR source [16].

136 The muonic hydrogen spectrum shows the importance of the Doppler-induced broadening  
 137 (Figure 14.3). A satisfactory description requires that about 2/3 of the  $\mu\text{H}$  atoms have kinetic  
 138 energies below a few eV contributing only to a negligible amount to the broadening. The  
 139 remaining 1/3 can be attributed to energies around 24 and 56 eV, which corresponds to the  
 140 Coulomb de-excitation transitions  $(5 - 4)$  and  $(4 - 3)$ . Within the uncertainties of such an  
 141 analysis, there is good agreement with cascade theory [8].

142 In pionic hydrogen, again a large fraction, about 60-80%, of the  $\pi\text{H}$  atoms have kinetic  
 143 energies below a few eV. The appearance of higher energies is needed to describe the line  
 144 shape. However, because of the hadronic broadening an assignment to particular Coulomb  
 145 de-excitation transitions is impossible [10].

146 It is worth mentioning that no Doppler contribution could be identified in pionic deuterium  
 147 within the experimental uncertainties [7]. A theoretical explanation for such behavior is pro-  
 148 vided by cascade theory [17].

149 The strong-interaction effects, summarized in Table 14.1, represent the weighted average  
 150 over the various transitions measured and target densities.

$\epsilon_{1s}^{\pi\text{H}}$	$\Gamma_{1s}^{\pi\text{H}}$	$\epsilon_{1s}^{\pi\text{D}}$	$\Gamma_{1s}^{\pi\text{D}}$
$(7085.8 \pm 9.6)$ [9]	$856 \pm 27$ [10]	$-2356 \pm 31$ [7]	$1171^{+23}_{-49}$ [7]

Table 14.1: Measured strong-interaction effects in pionic hydrogen and deuterium (in meV).

151 **14.5 Summary**

152 The three constraints on the two independent isoscalar and isovector  $\pi N$  scattering lengths  
 153 are shown in Figure 14.4. Because of the poor knowledge of LECs, the use of a modified  
 154 isoscalar scattering length  $\tilde{a}^+$  is more convenient in the constraint analyses. The most recent



155  $\chi$ PT calculation gives  $\tilde{a}^+ - a^+ = (-6.1 \pm 2.5) \cdot 10^{-3} m_\pi^{-1}$  [2]. It is important to note that good  
 156 overlap is achieved, although substantial chiral corrections have to be applied [2].

157 The precise result for the pion-production strength  $\alpha$  demonstrates the advantage of exotic  
 158 atoms, namely that the strong-interaction effects are determined without normalisation and  
 159 extrapolation. In Figure 14.5, the pionic- deuterium results are marked as the shaded area,  
 160 which is compared with pion-production experiments that typically specify statistical errors  
 161 only. The only theoretical approach yielding a reliable uncertainty is due to a  $\chi$ PT calculations  
 162 which, however, suffers at present from the scarce precision of some LECs [6].

$\tilde{a}^+$	$a^-$	$\alpha$
$(1.7 \pm 0.8) \cdot 10^{-3} m_\pi^{-1}$ [10]	$(86.6 \pm 1.0) \cdot 10^{-3} m_\pi^{-1}$ [10]	$251^{+5}_{-11}$ mb [7]

Table 14.2: Isoscalar and isovector scattering length  $\tilde{a}^+$  and  $a^-$  and threshold pion-production strength as derived from the strong-interaction effects in pionic hydrogen and deuterium.

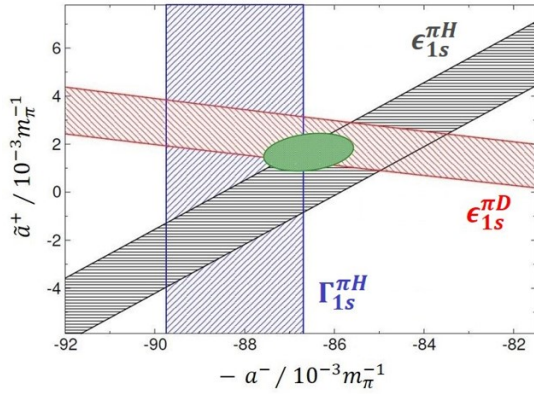


Figure 14.4: Constraints (bands) and combined result (ellipse) for the isoscalar and isovector  $\pi N$  scattering lengths  $\tilde{a}^+$  and  $a^-$  as derived from  $\epsilon_{1s}^{\pi H}$ ,  $\epsilon_{1s}^{\pi D}$ , and  $\Gamma_{1s}^{\pi H}$  [10].

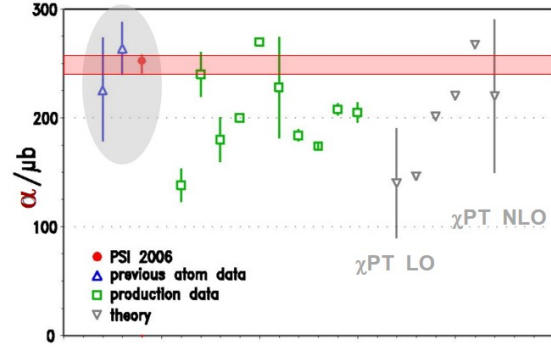


Figure 14.5: Comparison of results for pion-production strength  $\alpha$  at threshold on isoscalar  $NN$  pairs. The horizontal band represents the precision of the most recent result for  $\Gamma_{1s}^{\pi D}$  [7].

163 Exotic-atom data yield values for the reaction scattering lengths  $a_{\pi^- p \rightarrow \pi^- p}$  and  $a_{\pi^- p \rightarrow \pi^0 n}$   
 164 [9,10]. Applying the corrections provided by  $\chi$ PT calculations, as well  $a_{\pi^+ p \rightarrow \pi^+ p}$  as the isospin-  
 165 separated scattering lengths  $a_{1/2}$  and  $a_{3/2}$  are attainable [2,10]. The results are in very good  
 166 agreement with recent analyses of low-energy  $\pi N$  scattering data [18].

167 In summary, recent  $\pi H$ ,  $\pi D$ , and low-energy  $\pi N$  scattering data are quantitatively very  
 168 consistent when analysed within the framework of  $\chi$ PT.

## 169 References

- 170 [1] J. Gasser, V. Lyubovitzkij and A. Rusetski, "Hadronic atoms in QCD + QED", Phys. Rep.  
 171 456, 167 (2008).  
 172 [2] M. Hoferichter *et al.*, "Roy-steiner-equation analysis of pion-nucleon scattering", Phys.  
 173 Rep. 625, 1 (2016).

- 174 [3] D. Gotta, "Precision spectroscopy of light exotic atoms", Prog. Part. Nucl. Phys **52**, 133  
175 (2004).
- 176 [4] S. Deser *et al.*, "Energy level displacements in pi-mesonic atoms", Phys. Rev. **96**, 774  
177 (1954).
- 178 [5] V. Baru *et al.*, "Precision calculation of threshold  $\pi^-d$  scattering,  $\pi N$  scattering  
179 lengths, and the GMO sum rule", Nucl. Phys. A **872**, 69 (2011).
- 180 [6] V. Lensky *et al.*, "Towards a field theoretic understanding of  $\pi NN \rightarrow NN$ ", Eur. Phys.  
181 J. A **27**, 37 (2006).
- 182 [7] T. Strauch *et al.*, "Pionic deuterium", Eur. Phys. J. A **47**, 88 (2011).
- 183 [8] D. Covita *et al.*, "Line shape analysis of the  $K\beta$  transition in muonic hydrogen", Eur.  
184 Phys. J. D **72**, 72 (2018).
- 185 [9] M. Hennebach *et al.*, "Hadronic shift in pionic hydrogen", Eur. Phys. J. A **50**, 190  
186 (2014).
- 187 [10] A. Hirtl *et al.*, "Redetermination of the strong-interaction width in pionic hydrogen",  
188 to be published in Eur. Phys. J. A (2021).
- 189 [11] D. Gotta and L. Simons, "Remarks on a Johann spectrometer for exotic-atom research  
190 and more", Spectrochim. Acta B **120**, 9 (2016).
- 191 [12] N. Nelms *et al.*, "A large area CCD X-ray detector for exotic atom spectroscopy", Nucl.  
192 Instr. Meth. A **484**, 419 (2002).
- 193 [13] M. Trassinelli *et al.*, "Measurement of the charged pion mass using X-ray spectroscopy  
194 of exotic atoms", Phys. Lett. B **759**, 583 (2016).
- 195 [14] M. Daum and D. Gotta, "The mass of the  $\pi^-$ ", SciPost Phys. Proc. **2**, ppp (2021),  
196 doi:[10.21468/SciPostPhysProc.2.XXX](https://doi.org/10.21468/SciPostPhysProc.2.XXX).
- 197 [15] D. Gotta and L. Simons, "Cyclotron trap", SciPost Phys. Proc. **2**, ppp (2021),  
198 doi:[10.21468/SciPostPhysProc.2.XXX](https://doi.org/10.21468/SciPostPhysProc.2.XXX).
- 199 [16] D. Anagnostopoulos *et al.*, "On the characterisation of a Bragg spectrometer with  
200 X-rays from an ECR source", Nucl. Instr. and Meth. A **545**, 217 (2005).
- 201 [17] V. Popov and V. Pomerantsev, "The isotopic effect in the scattering and kinetics of the  
202 atomic cascade of excited  $\mu^-p$  and  $\mu^-d$  atoms", Phys. Rev. A **95**, 022506 (2017).
- 203 [18] J. Ruiz de Elvira *et al.*, "Extracting the  $\sigma$ -term from low-energy pion-nucleon scatter-  
204 ing", J. Phys. G **45**, 024001 (2018).